Chemosphere 286 (2022) 131943

Contents lists available at ScienceDirect

Chemosphere

journal homepage: www.elsevier.com/locate/chemosphere

Rapid removal of chloramphenicol via the synergy of *Geobacter* and metal oxide nanoparticles

Leilei Xiao [a,c], Fanghua Liu [a,c], P. Senthil Kumar [d], Yunwei Wei [b], Jian Liu [b,**], Dianfeng Han [e], Shangjie Shan [f], Xingyu Wang [f], Run Dang [f], Jiafeng Yu [b,*]

[a] CAS Key Laboratory of Coastal Environmental Processes and Ecological Remediation, Yantai Institute of Coastal Zone Research, Chinese Academy of Sciences, Yantai, 264003, China
[b] Shandong Key Laboratory of Biophysics, Institute of Biophysics, Dezhou University, Dezhou, 253023, PR China
[c] Key Laboratory of Coastal Biology and Biological Resources Utilization, Yantai Institute of Coastal Zone Research, Chinese Academy of Sciences, Yantai, 264003, PR China
[d] Department of Chemical Engineering, Sri Sivasubramaniya Nadar College of Engineering, Chennai, 603110, India
[e] Shandong Marine Resource and Environment Research Institute, Yantai, 264006, PR China
[f] Yantai University, Yantai, 264005, PR China

HIGHLIGHTS

- Fe_3O_4 and MnO_2 particles showed five times increase in chloramphenicol removal rate.
- Transcriptomic showed an increase of NADH-quinone oxidoreductase in two treatments.
- Fe_3O_4 and MnO_2 nanoparticles increased electron transfer efficiency.
- The primary enzymes for chloramphenicol reduction were different in three treatments.

GRAPHICAL ABSTRACT

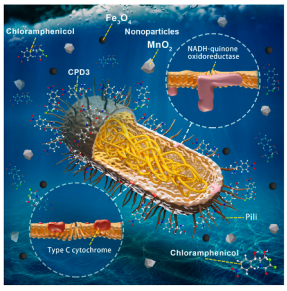

ARTICLE INFO

Handling editor: Chin Cheng.

Keywords:
Antibiotic
Nanoparticles
Dechlorination
MnO_2

ABSTRACT

The wide use of chloramphenicol and its residues in the environments are an increasing threat to human beings. Electroactive microorganisms were proven with the ability of biodegradation of chloramphenicol, but the removal rate and efficiency need to be improved. In this study, a model electricigens, *Geobacter metallireducens*, was supplied with and Fe_3O_4 and MnO_2 nanoparticles. Five times higher chloramphenicol removal rate (0.71 d^{-1}) and two times higher chloramphenicol removal efficiency (100%) was achieved. Fe_3O_4 and MnO_2 nanoparticles highly increased the current density and NADH-quinone oxidoreductase expression. Fe_3O_4 nanoparticles enhanced the expression of alcohol dehydrogenase and c-type cytochrome, while MnO_2 nanoparticles increased the transcription of pyruvate dehydrogenase and Type IV pili assembly genes. Chloramphenicol was

* Corresponding author. Shandong Key Laboratory of Biophysics, Institute of Biophysics, Dezhou University, No. 566 University Rd. West, Dezhou, 253023, PR China.
** Corresponding author. Shandong Key Laboratory of Biophysics, Institute of Biophysics, Dezhou University, No. 566 University Rd. West, Dezhou, 253023, PR China.
E-mail addresses: llxiao@yic.ac.cn (L. Xiao), fhliu@yic.ac.cn (F. Liu), senthilkumarp@ssn.edu.in (P.S. Kumar), sdweiyunwei@163.com (Y. Wei), liujian.cn@live.com (J. Liu), yantgongz@126.com (D. Han), ssjnb15866145316@163.com (S. Shan), lmy1500446388@163.com (X. Wang), xiaodang2333@163.com (R. Dang), jfyu1979@126.com (J. Yu).

https://doi.org/10.1016/j.chemosphere.2021.131943
Received 7 June 2021; Received in revised form 31 July 2021; Accepted 17 August 2021
Available online 20 August 2021

Fe_3O_4
Electron transfer

reduced to a type of dichlorination reducing product named CPD3 which is a benzene ring containing compound. Collectively, Fe_3O_4 and MnO_2 nanoparticles increased the chloramphenicol removal capacity in MFCs by enhancing electron transfer efficiency. This study provides new enhancing strategies for the bioremediation of chloramphenicol in the environments.

1. Introduction

Antibiotics are widely used to control infectious diseases in humans and animals. However, their residues are becoming an inevitable threat to human health. Chloramphenicol is the most used chlorinated nitroaromatic antibiotic and frequently be detected in many environments (Herraiz-Carboné et al., 2020; Xiao et al., 2021a). Even antibiotics can be removed by many physicochemical methods such as adsorption, advanced oxidation, and nanoparticles treatment (Herraiz-Carboné et al., 2020; Hu et al., 2020; Song et al., 2021; Yang et al., 2020b). The need for safe, effective, sustainable, and eco-friendly biodegradation methods is continuously increasing (Li et al., 2022).

Bioremediation technology based on microbial fuel cells (MFCs) was developed for organic compounds removal with the involvement of electroactive bacteria (EAB) (Wang et al., 2020). The *Geobacter* spp. is the most well-studied EAB family, and many bioremediation systems were established with them, such as the removal of monoaromatic hydrocarbons, chloramphenicol, tetracycline, hydrochloride, and polychlorinated biphenyls (Lu et al., 2021; Xiao et al., 2021b; Yang et al., 2020a, b, c). *Geobacter* spp is one of the most important electroactive bacteria which play a critical role in complex MFC systems. *Geobacter metallireducens* is a reprensentivte species of which the genome is fully sequenced. *Geobacter metallireducens* as one of the well-studied *Geobacter* was used for pollution removal, such as benzene (Zhang et al., 2013) and phenol (Sun et al., 2020). Our previous study reported the feasibility of using *Geobacter* species to degrade chloramphenicol (Xu et al., 2019; Xiao et al., 2021b). Therefore, we use *Geobacter metallireducens* as the model system in this study.

MFCs could remove antibiotics and produce electricity synchronously. Diverse factors affect the performance of MFCs, such as influent antibiotic concentration, hydraulic retention time (HRT), circuit operation mode (Zhang et al., 2018; Li et al., 2018, 2020). Long HRT showed better MFC performance (Wen et al., 2020; Song et al., 2018). MFCs-based bioremediation technology suffered from low removal rates and efficiency due to the toxic effects of antibiotics on functional microbes. Conductive materials could improve the biodegradation capacity by enhancing microbial electron transfer efficiency among different species (Tang et al., 2020; Xiao et al., 2019a, 2020a) or within pure cultures (Sun et al., 2020; Liu et al., 2021). Our recent research proposed a synergic treatment of *G. sulfurreducens* with electric fields to enhance the removal efficiency of chloramphenicol (Xiao et al., 2021b). However, achieving beneficial industrial efficiency was the main challenge for the bioremediation of antibiotics, and the microbial mechanism is still unclear.

Nanoparticles with special electrochemical properties could affect the performance of MFCs by improving the electron transfer efficiency or simply serving as electron acceptors (Xiao et al., 2019b, 2020b, 2020b; Tang et al., 2020; Li et al., 2019; Tuntoolavest and Burgos, 2005). Fe_3O_4 and MnO_2 nanoparticles were feasible materials to enhance MFCs activity, for example, to stimulate methane production or nitrification activity (Liu et al., 2020; Thatikayala et al., 2021; Xiao et al., 2018), but potential effects on chloramphenicol removal are unclear. This study aims to investigate the effect of Fe_3O_4 and MnO_2 nanoparticles on the removal of chloramphenicol by *G. metallireducens* and unveil the underlying mechanism. The removal dynamics were evaluated and the electrochemical behavior of *G. metallireducens* with Fe_3O_4 and MnO_2 nanoparticles was characterized by cyclic voltammetry (CV) and differential pulse voltammetry (DPV). The differential gene expression of *G. metallireducens* respond to Fe_3O_4 and MnO_2 nanoparticles was revealed by transcriptomic analysis. These findings will promote the application of EAB for chloramphenicol removal.

2. Materials and methods

2.1. Preparation and characterization of metal oxide nanoparticles

$FeCl_3{\cdot}6H_2O$ (99%), sodium acetate (99%), ethylene glycol (EG, 98%), and polyethylene glycol (average molecular weight 2000) were purchased from Shanghai Macklin Biochemical Co., Ltd. MnO_2 nanoparticles were purchased from Beijing Deke Daojin Science and Technology Co., Ltd. Deionized water was prepared with a Milli-Q water purification system (LCT-I-10/20T). All reagents were analytical grade and used as received without further purification.

The Fe_3O_4 nanoparticles were prepared by a solvothermal method (Deng et al., 2005). In a typical synthesis, 5.06 g $FeCl_3{\cdot}6H_2O$ was dissolved in 150 mL ethylene glycol under vigorous stirring at room temperature. Afterwards, 13.5 g sodium acetate and 3.75 g polyethylene glycol were added into the above solution, respectively. The mixture was stirred vigorously for 1 h and then sealed in an autoclave and maintained at 200 °C for 10 h. Subsequently, the as-synthesized Fe_3O_4 nanoparticles were collected via centrifugation and washed repeatedly with alcohol for three times, and dried at 60 °C overnight.

X-ray diffraction (XRD) patterns were recorded on a Bruker D8 ADVANCE X-ray diffractometer with Cu Kα radiation ($\lambda = 1.5418$ Å) by depositing the product on a glass slide. The morphologies of the products were characterized by transmission electron microscopy (TEM, JEOL JEM-2100) employing an accelerating voltage of 200 kV. The samples for TEM observations were prepared by putting the products on a thin carbon film coated copper grids. Scanning electron microscope (SEM) and energy-dispersive X-ray (EDX) elemental mapping were carried out on ZEISS MERLIN Compact.

2.2. Bacterial strains and growth conditions

The cultivation of *G. metallireducens* GS-15 (ATCC 53774/DSM 7210) was previously described in Xu et al. (2019). In brief, fresh inoculations of the strain in freshwater-acetate medium (DR and EJ, 1988) with 30 mM acetate and 20 mM nitrate were kept anaerobically at 30 °C in the dark for more than four days to reach a stationary phase.

2.3. Degradation of chloramphenicol by G. metallireducens

Cultures at the stationary phase were supplied with 40 mg/L chloramphenicol in 100 mL serum bottles with a working volume of 40 mL. Three experiment conditions were set: *G. metallireducens* culture (control), *G. metallireducens* culture supplied with Fe_3O_4 nanoparticles at a concentration of 0.35 g Fe per liter, and *G. metallireducens* culture supplied with MnO_2 nanoparticles at a concentration of 0.35 g Mn per liter. During the chloramphenicol removal experiments, samples were withdrawn in an anaerobic glovebox sparged with N_2:H_2 (95:5) (v:v) mixed gas. All the experiments were conducted in triplicates.

2.4. Characterization of G. metallireducens by electrochemical methods

The methods of CV and DPV in a conventional three-electrode electrochemical cell (CHI660 electrochemical workstation, Chenhua, China) were performed to assess the electrochemical activity of *G. metallireducens* for chloramphenicol reduction. The working electrode

was a glassy carbon electrode (Φ = 3 mm), the counter electrode was a Pt sheet electrode, and the reference electrode was an Ag/AgCl electrode. Prior to the experiment, the glassy carbon electrode was polished with 0.3 and 0.05 μm alumina slurries for 3 min, rinsed with ultrapure water for 3min, sonicated in ultrapure water and ethanol for 3 min, and dried under an infrared lamp environment. CV measurement was conducted in the phosphate buffered solution containing 40 mg/L chloramphenicol and *G. metallireducens* (OD_{540} = 0.2) with or without Fe_3O_4/MnO_2 nanoparticles at a scanning rate of 5 mV between −1 V and 1 V. DPV measurement was performed at a scanning rate of 5 mV/s between −1 V and 1 V.

2.5. Analytical methods

The concentration of chloramphenicol was determined using high-performance liquid chromatography (HPLC, 1260 Infinity, Agilent, USA) with a PDA detector. Samples were taken every 24 h and filtered over 0.22 μm filters prior to HPLC analysis. The separation was performed using a C18 column. The flow rate of the mobile phase (methanol: water, 65:35, v/v) was 1 mL/min, and the detection wavelength was 275 nm.

The reduction products were extracted from the medium by solid-phase extraction using Waters HLB Oasis® SPE cartridges and then identified by liquid chromatography-mass spectrometry (LC-MS, LCQ Fleet ion trap mass spectrometer, Thermo Fisher, USA), which was equipped with an electrospray ionization source and operated in positive/negative polarity mode. The column and detection conditions were the same as mentioned above.

2.6. Transcriptomic analysis

The samples of *G. metallireducens* at day two were collected for transcriptomic analysis. Total RNA was extracted using the RNeasy Mini Kit (Qiagen, Germany) following the manufacturer's manual. The quality and quantity were determined using an Agilent 2100 Bioanalyzer (Agilent Technologies, Palo Alto, USA). 1 μg of high-quality RNA of each sample was subjected to library construction following the instruction of the NEBNext® Ultra™ RNA Library Prep Kit for Illumina (NEB, USA). The libraries were sequenced on an Illumina HiSeq platform producing paired-end reads results.

The raw reads were quality filtered by Trimmomatic (v0.40) and aligned to the reference genome obtained from NCBI (GCF_000012925.1) by HISAT2 (Kim et al., 2019). Then the quantification of the transcripts was calculated by StringTie (v2.1.3). The statistical analysis was performed with R (v4.0.3). The KEGG pathway enrichment analysis was conducted using the clusterProfiler (v4.0.0) R package.

3. Results and discussion

3.1. Characterization of high purity Fe_3O_4 and MnO_2 nanoparticles

The XRD patterns were carried out to reveal the crystallographic structure of the as-prepared Fe_3O_4 and MnO_2 nanoparticles. The patterns can be easily indexed to Fe_3O_4 (JCPDS no.19-0629) and MnO_2 (JCPDS no.24-0735) (Fig. 1a). Meanwhile, no impurity was detected from the XRD spectrum, indicating that the Fe_3O_4 and MnO_2 nanoparticles could be obtained by the current synthetic system with high purity. Subsequently, the size, morphology, and elemental-mapping of Fe_3O_4 and MnO_2 nanoparticles were investigated by TEM and SEM. As

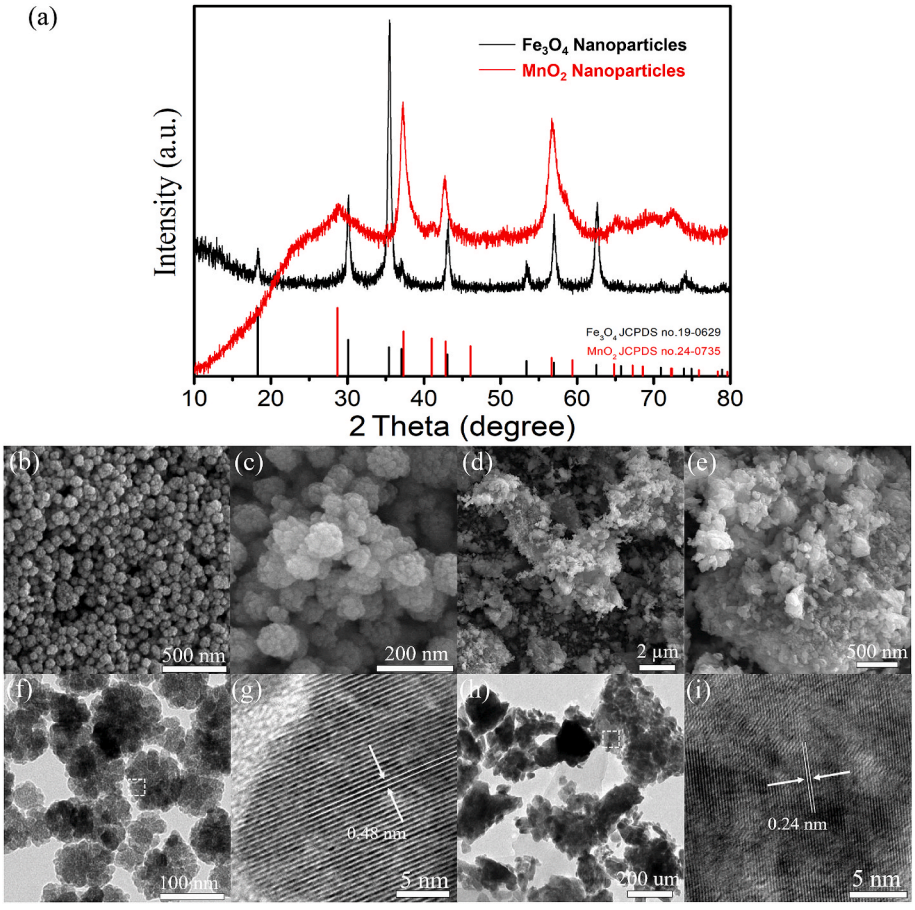

Fig. 1. Characterization of Fe_3O_4 and MnO_2 nanoparticles. (a) XRD patterns of the Fe_3O_4 (black) and MnO_2 (red) nanoparticles. (b–c) Low- and high-magnification SEM images of the Fe_3O_4 nanoparticles. (d–e) Low- and high-magnification SEM images of the MnO_2 nanoparticles. (f–g) TEM and HRTEM images of the Fe_3O_4 nanoparticles. (h–i) TEM and HRTEM images of the MnO_2 nanoparticles. (For interpretation of the references to color in this figure legend, the reader is referred to the Web version of this article.)

shown in Fig. 1b–i, the as-synthesized Fe_3O_4 nanoparticles were with the size between 50 and 100 nm, while the major product of MnO_2 nanoparticles was large agglomerates composed of random-shaped nanoparticles range from 50 to 200 nm. The size and shape of the materials we obtained were similar to previous studies (Song et al., 2019; Thatikayala et al., 2021; Xing et al., 2020), indicating a good quality. Furthermore, HRTEM images in Fig. 1e and i demonstrated that the adjacent lattice fringes of 0.48 nm were well indexed to the lattice spacing of (111) plane of Fe_3O_4. The adjacent lattice fringes measured from the MnO_2 nanoparticles were 0.24 nm, which corresponded to the lattice spacing of (101) planes of MnO_2. To further investigate the elemental distribution of Fe and Mn in the as-prepared Fe_3O_4 and MnO_2 nanoparticles, elemental mappings were collected and shown in Figure S1. It can be clearly observed that Fe and Mn elements were evenly distributed throughout the entire samples.

3.2. Fe_3O_4 and MnO_2 nanoparticles enhanced chloramphenicol removal

We tested the chloramphenicol removal dynamics of *G. metallireducens* supplied with Fe_3O_4 and MnO_2 nanoparticles (Fig. 2). Both highly increased chloramphenicol removal efficiency, where chloramphenicol was eliminated entirely. By comparison, *G. metallireducens* pure culture reduced only half of the original chloramphenicol. Guo et al. (2020) tested the effect of Fe_3O_4 nanoparticles on the concentration of chloramphenicol and found that less than 10% was absorbed by Fe_3O_4. Moreover, the results of Deng et al. (2017) showed that less than 7% of ciprofloxacin was absorbed by MnO_2 nanoparticles. Considering that the removal efficiency was 100% in this study, the absorption of Fe_3O_4 and MnO_2 nanoparticles may be weakly contributing.

Interestingly, Fe_3O_4 and MnO_2 nanoparticles not only increased the removal efficiency but also accelerated the reduction rate. Within only three days, the chloramphenicol in the system was almost completely reduced. We calculated the chloramphenicol reducing rate constant by fitting the following formula:

$$\ln(\frac{C}{C_0}) = -k_{app}t \quad (1)$$

where C and C_0 are the real-time concentration and the initial concentration, respectively, k_{app} is the apparent rate constant, and t is the reaction time.

The apparent chloramphenicol removal rate constant of *G. metallireducens* was 0.16 d^{-1}. On the contrary, the constant was 0.718 d^{-1} and 0.713 d^{-1} for Fe_3O_4 and MnO_2 nanoparticles, respectively, which were almost 5 times higher than the pure culture. Jiang et al. (2019) showed that conductive nanoparticles could increase the electron transfer efficiency within MFCs, which increased the redox activity in *G. metallireducens* and resulted in a rapid chloramphenicol removal rate. As chloramphenicol was rapidly removed from the culture, its inhibition effect on the growth of *G. metallireducens* was relieved, and subsequently, the removal efficiency was increased.

Conductive materials have been wildly used in MFC practices. In most cases, they could enhance the performance through increasing electron transfer (Mukherjee and Saravanan, 2020; Wang et al., 2020). Other properties of these materials such as absorption, immobilization could also promote the performance (Lu et al., 2020; He et al., 2020; Xiao et al., 2021c). Even here we only used metal oxide, other conductive materials such as biochar, carbon nanotube, graphene (Huang et al., 2019; Wang et al., 2020; Xiao et al., 2019b, 2021d) could also promote the efficiency of electron transfer and potential CAP removal.

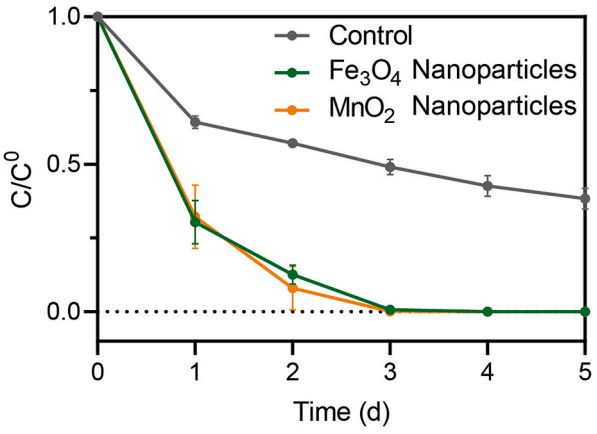

Fig. 2. Chloramphenicol reduction by *G. metallireducens*. The initial concentration was 40 mgL^{-1}. The Fe_3O_4 and MnO_2 nanoparticles group was *G. metallireducens* culture supplied with Fe_3O_4 or MnO_2 nanoparticles, respectively. The control group was *G. metallireducens* culture only.

3.3. Electrochemical analysis of *G. metallireducens* with Fe_3O_4 and MnO_2 nanoparticles

Cyclic voltammetry (CV) and differential pulse voltammetry (DPV) were performed to assess the electrochemical property of *G. metallireducens* with Fe_3O_4 and MnO_2 nanoparticles during chloramphenicol reduction. Chloramphenicol reduction had a characteristic peak at around −0.6 V (vs. Ag/AgCl) (Mao et al., 2018), which was also observed in pure *G. metallireducens* culture (Fig. 3a). On the contrary, no peak was observed with Fe_3O_4 nanoparticles and a light peak with MnO_2 nanoparticles. This phenomenon was often observed in MFCs with conductive nanoparticles (Mukherjee and Saravanan, 2020; Wang et al., 2020), where these materials accelerated the electron transfer efficiency and led to a smooth CV curve.

Interestingly, the current density with Fe_3O_4 and MnO_2

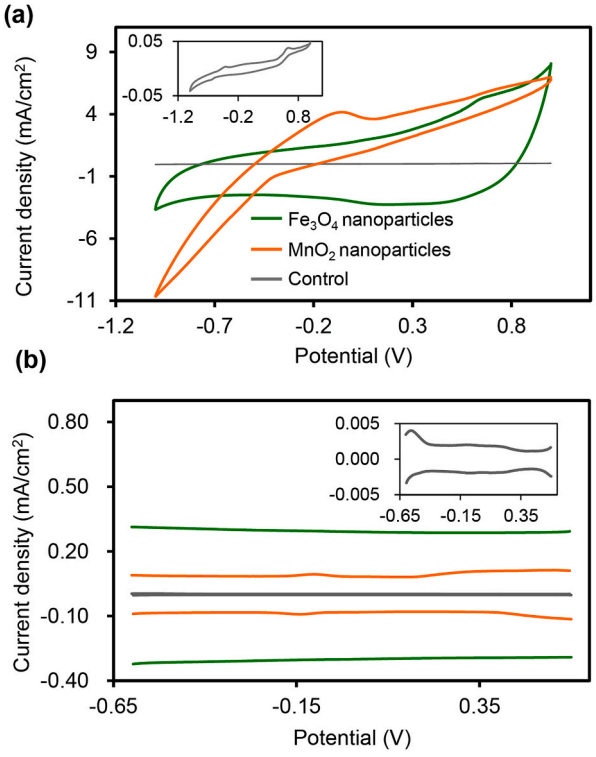

Fig. 3. Cyclic voltammograms analysis (a) and differential pulse voltammetry analysis (b) of *G. metallireducens* (grey) with Fe_3O_4 (green) or MnO_2 nanoparticles (orange). (For interpretation of the references to color in this figure legend, the reader is referred to the Web version of this article.)

nanoparticles was hundreds of times higher than the control group in both CV and DPV analysis (Fig. 3). Addition of conductive materials shifted the electrochemical property of the entire system (Li et al., 2018; Li et al., 2019; Teymourian et al., 2013), which may substantially change the redox status in the cell and enhance the global degradation metabolism by enhancing electron transfer efficiency (Jiang et al., 2019).

3.4. Transcriptomic analysis of the strengthening mechanism

Comparing to control group, Fe_3O_4 nanoparticles induced 206 genes and suppressed 139 genes, while MnO_2 nanoparticles induced 2117 genes and suppressed 96 genes (Fig. 4a, Table S1). We performed KEGG pathway enrichment analysis on differentially expressed genes. We found that both Fe_3O_4 and MnO_2 nanoparticles induced toluene and aromatic compounds degradation pathway (Table 1). It suggested that a potential pathway for chloramphenicol degradation was impacted by nanoparticles.

Type IV pili were conductive and crucial for extracellular electron transfer (Malvankar et al., 2014). A very recent study showed that Fe_3O_4 nanoparticles could act as a conductive structure and compensated for the function of Type IV pili (Cavalcante et al., 2021). However, the expression of Type IV pili genes was not obviously affected by Fe_3O_4 nanoparticles in this study (Fig. 4b). On the contrary, more than 80% of the Type IV pili genes were significantly up-regulated in the MnO_2 nanoparticles treatment, showing that MnO_2 nanoparticles interacted with Type IV pili to increase electron transfer efficiency. All the c-type cytochrome genes were up-regulated in the Fe_3O_4 nanoparticles treatment, but only one of them was increased in the MnO_2 nanoparticles treatment.

C-type cytochrome mainly localized onto the outer membrane and participated in the electron transfer chain (Ueki, 2021). Therefore, we speculated that Fe_3O_4 nanoparticles interacted with cytochrome *c* to increase electron transfer efficiency. Fe_3O_4 and MnO_2 nanoparticles both induced part of the NADH-quinone oxidoreductase, a crucial protein for energy transduction and electron transfer (Zheng et al., 2020). Fe_3O_4 and MnO_2 nanoparticles may also accelerate electron transfer in the cells by enhancing cellular respiration.

Table 1
Pathway enrichment of DEGs.

KEEG Term	Group	Rich_ratio	q-value
Toluene degradation	Fe_3O_4 nanoparticles	0.0625	0.0032180
	MnO_2 nanoparticles	0.022109	0.0055899
Degradation of aromatic compounds	Fe_3O_4 nanoparticles	0.080357	0.0032180
	MnO_2 nanoparticles	0.028912	0.0489792
Nitrogen metabolism	Fe_3O_4 nanoparticles	0.080357	0.0064687
Oxidative phosphorylation	Fe_3O_4 nanoparticles	0.133929	0.0139444
Microbial metabolism in diverse environments	Fe_3O_4 nanoparticles	0.303571	0.0408405
Two-component system	MnO_2 nanoparticles	0.142857	0.0000563
Bacterial chemotaxis	MnO_2 nanoparticles	0.083333	0.0000563
Flagellar assembly	MnO_2 nanoparticles	0.04932	0.0045635

Moreover, the expression of the alcohol dehydrogenase gene (Gmet 1046), which can degrade chloroalkane-like substrate (Das et al., 2015) was highly up-regulated in the Fe_3O_4 nanoparticles treatment but not in the MnO_2 nanoparticles treatment. On the contrary, MnO_2 nanoparticles induced the pyruvate dehydrogenase (Gmet_2511), indicating that the primary chloramphenicol degrading enzymes were different in the two treatments (Figure S2).

3.5. Chloramphenicol reduction products

We applied HPLC-MS/MS analysis to determine the intermediate products during the reduction of chloramphenicol. In the control group (Fig. 5a), we could identify the typical peak at 321, 323, and 325 m/z for chloramphenicol (Xiao et al., 2021b), while none of these peaks were observed in the Fe_3O_4 and MnO_2 nanoparticles group (Fig. 5b). A higher degradation efficiency was obtained in the presence of nanoparticles.

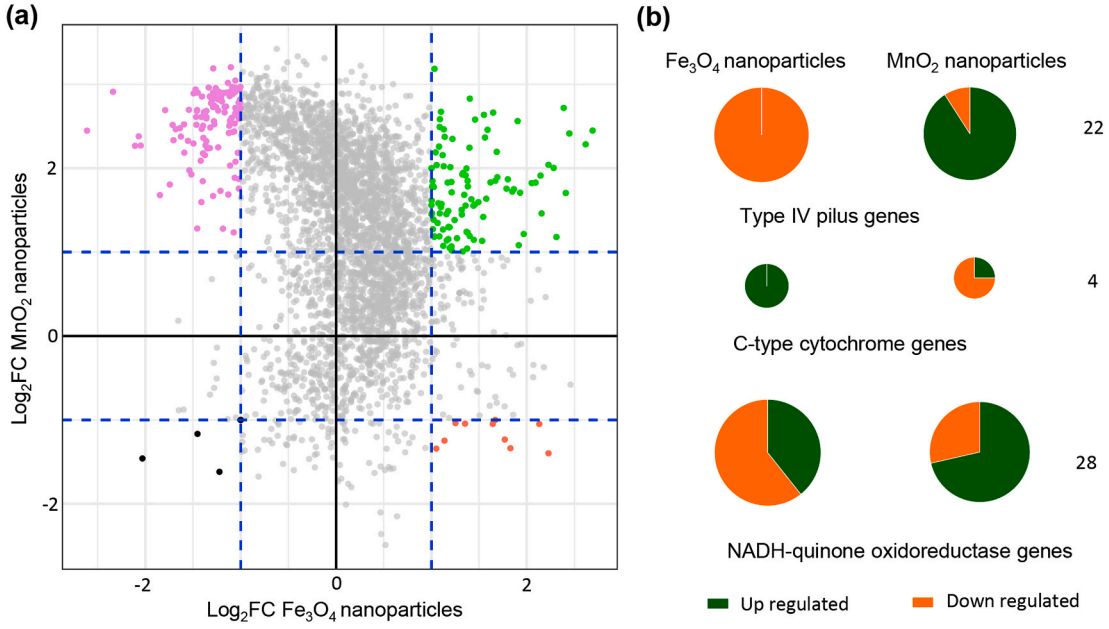

Fig. 4. Transcriptome analysis. (a) The plot of the log_2FC value of Fe_3O_4 nanoparticles vs Control (x-axis) and MnO_2 nanoparticles vs Control (y axis). Dashed blue line showed the threshold of 2 times fold change. (b) Chloramphenicol reducing related genes. The size of the cycle showed the total number of genes (denoted on the right side). Color green denoted upregulated genes and color orange denoted genes not significantly change. None of these genes were downregulated. (For interpretation of the references to color in this figure legend, the reader is referred to the Web version of this article.)

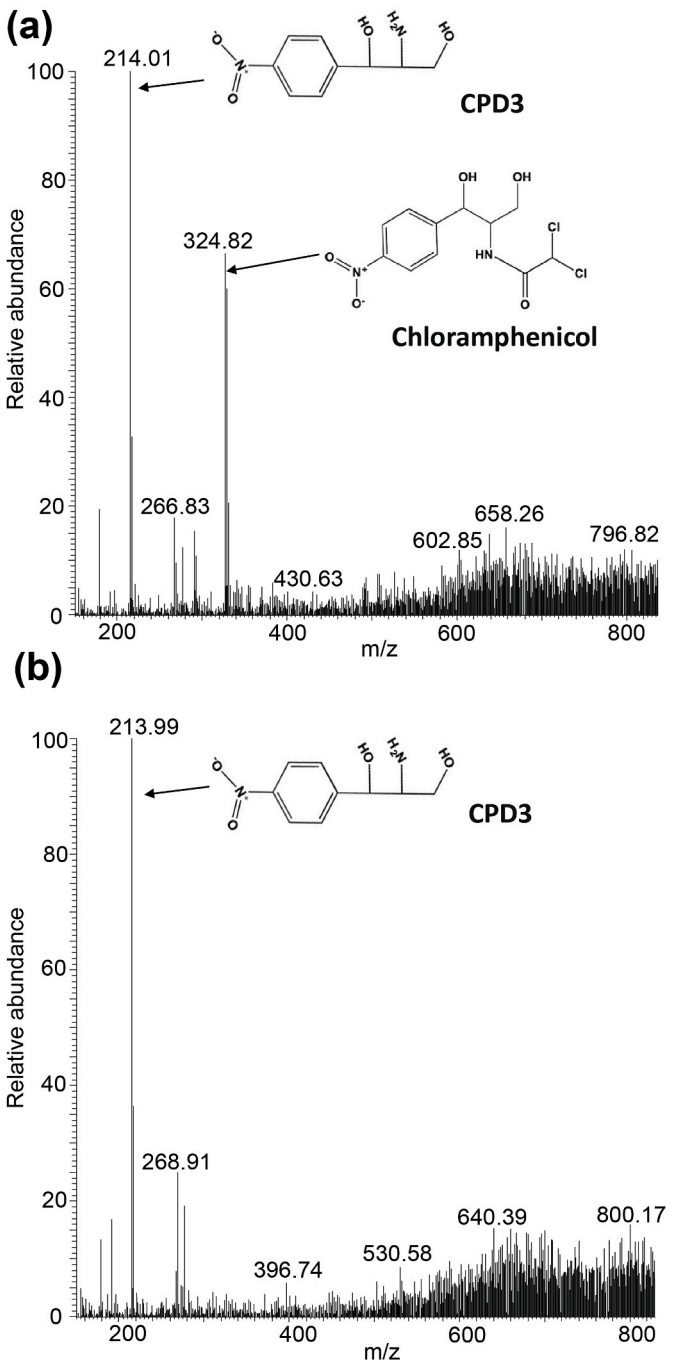

Fig. 5. The potential reduction products of chloramphenicol. (a) control group. (b) Fe_3O_4 nanoparticles group, and (c) MnO_2 nanoparticles group.

The most well-studied reduction path of chloramphenicol was chloramphenicol → AMCl2 (295 m/z) → AMCl (279 m/z) → AM (247 m/z) (Smith et al., 2007; Yan et al., 2019). However, none of these peaks were prominent in the mass spectrum of all three groups. Instead, one peak at 214 m/z with high abundance was observed, which was an intermediate product named CPD3 , a benzene ring containing compound ($C_9H_{12}N_2O_4$), during thermal degradation (Tian and Bayen, 2018). Comparing with our previous study (Xu et al., 2019), the sampling time was later, and the CAP residues (12 ± 5%) were less in the current study (previously 38 ± 7%). Therefore, CAP may be degraded more thoroughly to CPD3, instead of AMCl2 and AMCL. Therefore, conductive nanoparticles improved degradation efficiency but did not change the degradation pathway (Fig. 6).

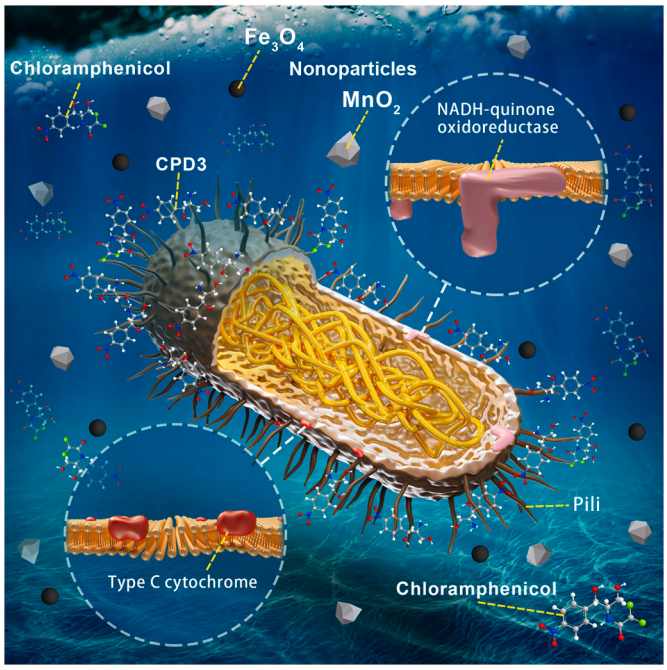

Fig. 6. The concept of chloramphenicol reduction to CPD3 by *G. metallireducens* in the presence of Fe_3O_4 and MnO_2 nanoparticles.

4. Conclusion

In the study, we showed a procedure completed chloramphenicol degradation to a dichlorination reducing product CPD3 in *G. metallireducens*. Nano-scale Fe_3O_4 and MnO_2 enhanced chloramphenicol removal rate (five times) and removal efficiency (two times) by accelerating the electron transfer efficiency. Fe_3O_4 and MnO_2 nanoparticles induced the NADH-dependent electron transfer chain. Fe_3O_4 nanoparticles used alcohol dehydrogenase as the primary enzymes for chloramphenicol reduction and cytochrome *c* as electron transduction proteins while MnO_2 nanoparticles used pyruvate dehydrogenase as the primary enzymes for chloramphenicol reduction and e-pili as electron transduction proteins (Figure S2). Although the efficiency of this system is high, but the degradation product was still large and toxic and the interactions between nanoparticles and the microbe were unclear. Other techniques should be applied to completely decompose CAP to non-toxic small molecules such as CO_2 and H_2O.

Credit author statement

Leilei Xiao: Conceptualization, Methodology, Visualization, Formal analysis, Data Curation, Writing - Original Draft, Funding acquisition. Fanghua Liu: Validation, Resources, Formal analysis, Yunwei Wei: Investigation, Data Curation, Jian Liu: Methodology, Visualization, Formal analysis, Data Curation, Writing - Original Draft, P. Senthil Kumar: Visualization, Data Curation, Writing - Review & Editing, Dianfeng Han: Investigation, Data Curation, Shangjie Shan: Investigation, Data Curation, Xingyu Wang: Investigation, Data Curation, Run Dang: Investigation, Data Curation, Jiafeng Yu: Conceptualization, Methodology, Supervision, Funding acquisition.

Declaration of competing interest

The authors declare that they have no known competing financial interests or personal relationships that could have appeared to influence the work reported in this paper.

Acknowledgments

This work was supported by the National Natural Science Foundation of China (61771093, 42077025, U20A20109, 62011530044), Youth Innovation Promotion Association, CAS (2021213), the Youth Science and technology innovation plan of universities in Shandong (2019KJE007), and Natural Science Foundation of Shandong Province (ZR2016JL027).

Appendix A. Supplementary data

Supplementary data to this article can be found online at https://doi.org/10.1016/j.chemosphere.2021.131943.

References

Cavalcante, W.A., Gehring, T.A., Zaiat, M., 2021. Stimulation and inhibition of direct interspecies electron transfer mechanisms within methanogenic reactors by adding magnetite and granular actived carbon. Chem. Eng. J. https://doi.org/10.1016/j.cej.2021.128882.

Das, D., Baruah, R., Sarma Roy, A., Singh, A.K., Deka Boruah, H.P., Kalita, J., Bora, T.C., 2015. Complete genome sequence analysis of *Pseudomonas aeruginosa* N002 reveals its genetic adaptation for crude oil degradation. Genomics 105, 182–190. https://doi.org/10.1016/j.ygeno.2014.12.006.

Deng, H., Li, X., Peng, Q., Wang, X., Chen, J., Li, Y., 2005. Monodisperse magnetic single-crystal ferrite microspheres. Angew. Chem. Int. Ed. 44, 2782–2785. https://doi.org/10.1002/anie.200462551.

DR, L., EJ, P., 1988. Novel mode of microbial energy metabolism: organic carbon oxidation coupled to dissimilatory reduction of iron or manganese. Appl. Environ. Microbiol. 54, 1472–1480. https://doi.org/10.1128/aem.54.6.1472-1480.1988.

He, P.J., Zhang, H.H., Duan, H.W., Shao, L.M., Lu, F., 2020. Continuity of biochar-associated biofilm in anaerobic digestion. Chem. Eng. J. 390, 124605. https://doi.org/10.1016/j.cej.2020.124605.

Herraiz-Carboné, M., Cotillas, S., Lacasa, E., Moratalla, Á., Cañizares, P., Rodrigo, M.A., Sáez, C., 2020. Improving the biodegradability of hospital urines polluted with chloramphenicol by the application of electrochemical oxidation. Sci. Total Environ. 725, 138430. https://doi.org/10.1016/j.scitotenv.2020.138430.

Hu, X., Deng, Y., Zhou, J., Liu, B., Yang, A., Jin, T., Fai Tsang, Y., 2020. N- and O self-doped biomass porous carbon cathode in an electro-Fenton system for chloramphenicol degradation. Separ. Purif. Technol. 251, 117376. https://doi.org/10.1016/j.seppur.2020.117376.

Huang, D., Wu, J., Wang, L., Liu, X., Meng, J., Tang, X., Tang, C., Xu, J., 2019. Novel insight into adsorption and co-adsorption of heavy metal ions and an organic pollutant by magnetic graphene nanomaterials in water. Chem. Eng. J. 358, 1399–1409. https://doi.org/10.1016/j.cej.2018.10.138.

Jiang, Y., Xi, B., Li, R., Li, M., Xu, Z., Yang, Y., Gao, S., 2019. Advances in Fe(III) bioreduction and its application prospect for groundwater remediation: a review. Front. Environ. Sci. Eng. https://doi.org/10.1007/s11783-019-1173-9.

Kim, D., Paggi, J.M., Park, C., Bennett, C., Salzberg, S.L., 2019. Graph-based genome alignment and genotyping with HISAT2 and HISAT-genotype. Nat. Biotechnol. 37, 907–915. https://doi.org/10.1038/s41587-019-0201-4.

Li, H., Song, H.L., Yang, X.L., Zhang, S., Yang, Y.L., Zhang, L.M., Xu, H., Wang, Y.W., 2018. A continuous flow MFC-CW coupled with a biofilm electrode reactor to simultaneously attenuate sulfamethoxazole and its corresponding resistance genes. Sci. Total Environ. 637 (638), 295–305. https://doi.org/10.1016/j.scitotenv.2018.04.359.

Li, Y., Ma, Y., Lichtfouse, E., Song, J., Gong, R., Zhang, J., Wang, S., Xiao, L., 2022. In situ electrochemical synthesis of Ggraphene-poly(arginine) composite for p-nitrophenol monitoring. J. Hazard Mater. 421, 126718. https://doi.org/10.1016/j.jhazmat.2021.126718.

Li, Y., Ren, C., Zhao, Zisheng, Yu, Q., Zhao, Zhiqiang, Liu, L., Zhang, Y., Feng, Y., 2019. Enhancing anaerobic degradation of phenol to methane via solubilizing Fe(III) oxides for dissimilatory iron reduction with organic chelates. Bioresour. Technol. 291, 121858. https://doi.org/10.1016/j.biortech.2019.121858.

Li, J., Xiao, L., Zheng, S., Zhang, Y., Luo, M., Tong, C., Xu, H., Tan, Y., Liu, J., Wang, O., Liu, F., 2018. A new insight into the strategy for methane production affected by conductive carbon cloth in wetland soil: Beneficial to acetoclastic methanogenesis instead of CO_2 reduction. Sci. Total Environ. 643, 1024–1030. https://doi.org/10.1016/j.scitotenv.2018.06.271.

Li, H., Xu, H., Song, H.L., Lu, Y., Yang, X.L., 2020. Antibiotic resistance genes, bacterial communities, and functions in constructed wetland-microbial fuel cells: responses to the co-stresses of antibiotics and zinc. Environ. Pollut. 265, 115084. https://doi.org/10.1016/j.envpol.2020.115084.

Liu, H., Zhang, Y., Zhou, Y., Chen, Z., Lichtfouse, E., 2020. Self-provided microbial electricity enhanced wastewater treatment using carbon felt anode coated with amino-functionalized Fe_3O_4. J. Water Process. Eng. 38, 101649. https://doi.org/10.1016/j.jwpe.2020.101649.

Liu, J., Liu, F., Yu, J., Wang, Q., Li, Z., Liu, K., Xu, C., Yu, H., Xiao, L., 2021. Proteomics reveal biomethane production process induced by carbon nanotube. Environ. Res. 200, 111417. https://doi.org/10.1016/j.envres.2021.111417.

Lu, J.S., Chang, J.S., Lee, D.J., 2020. Adding carbon-based materials on anaerobic digestion performance: a mini-review. Bioresour. Technol. 300, 122696. https://doi.org/10.1016/j.biortech.2019.122696.

Lu, Q., Liu, J., He, H., Liang, Z., Qiu, R., Wang, S., 2021. Waste activated sludge stimulates in situ microbial reductive dehalogenation of organohalide-contaminated soil. J. Hazard Mater. 411, 125189. https://doi.org/10.1016/j.jhazmat.2021.125189.

Malvankar, N.S., Yalcin, S.E., Tuominen, M.T., Lovley, D.R., 2014. Visualization of charge propagation along individual pili proteins using ambient electrostatic force microscopy. Nat. Nanotechnol. 9, 1012–1017. https://doi.org/10.1038/nnano.2014.236.

Mao, Y., Guo, L., Ning, X., Li, J., Zheng, J., 2018. The signal amplification in electrochemical detection of chloramphenicol using sulfonated polyaniline-chitosan composite as redox capacitor. Electroanalysis 30, 2085–2093. https://doi.org/10.1002/elan.201800218.

Mukherjee, P., Saravanan, P., 2020. Graphite nanopowder functionalized 3-D acrylamide polymeric anode for enhanced performance of microbial fuel cell. Int. J. Hydrogen Energy 45, 23411–23421. https://doi.org/10.1016/j.ijhydene.2020.06.110.

Smith, A.L., Erwin, A.L., Kline, T., Unrath, W.C.T., Nelson, K., Weber, A., Howald, W.N., 2007. Chloramphenicol is a substrate for a novel nitroreductase pathway in Haemophilus influenzae. Antimicrob. Agents Chemother. 51, 2820–2829. https://doi.org/10.1128/AAC.00087-07.

Song, H.L., Li, H., Zhang, S., Yang, Y.L., Zhang, L.M., Xu, H., Yang, X.L., 2018. Fate of sulfadiazine and its corresponding resistance genes in up-flow microbial fuel cell coupled constructed wetlands: effects of circuit operation mode and hydraulic retention time. Chem. Eng. J. 350, 920–929. https://doi.org/10.1016/j.cej.2018.06.035.

Song, X., Liu, J., Jiang, Q., Zhang, P., Shao, Y., He, W., Feng, Y., 2019. Enhanced electron transfer and methane production from low-strength wastewater using a new granular activated carbon modified with nano-Fe_3O_4. Chem. Eng. J. 374, 1344–1352. https://doi.org/10.1016/j.cej.2019.05.216.

Song, X., Zhang, H., Bian, Z., Wang, H., 2021. In situ electrogeneration and activation of H_2O_2 by atomic Fe catalysts for the efficient removal of chloramphenicol. J. Hazard Mater. 412, 125162. https://doi.org/10.1016/j.jhazmat.2021.125162.

Sun, C., Yu, Q., Zhao, Z., Zhang, Y., 2020. Syntrophic metabolism of phenol in the anodic degradation within a Phenol-Cr(VI) coupled microbial electrolysis cell. Sci. Total Environ. 723, 137990. https://doi.org/10.1016/j.scitotenv.2020.137990.

Tang, Y., Li, Y., Zhang, M., Xiong, P., Liu, L., Bao, Y., Zhao, Z., 2020. Link between characteristics of Fe(III) oxides and critical role in enhancing anaerobic methanogenic degradation of complex organic compounds. Environ. Res. 110498. https://doi.org/10.1016/j.envres.2020.110498.

Teymourian, H., Salimi, A., Khezrian, S., 2013. Fe_3O_4 magnetic nanoparticles/reduced graphene oxide nanosheets as a novel electrochemical and bioeletrochemical sensing platform. Biosens. Bioelectron. 49, 1–8. https://doi.org/10.1016/j.bios.2013.04.034.

Thatikayala, D., Pant, D., Min, B., 2021. MnO_2/reduced graphene oxide nanohybrids as a cathode catalyst for the microbial reduction of CO_2 to acetate and isobutyric acid. Sustain. Energy Technol. Assess. 45, 101114. https://doi.org/10.1016/j.seta.2021.101114.

Tian, L., Bayen, S., 2018. Thermal degradation of chloramphenicol in model solutions, spiked tissues and incurred samples. Food Chem. 248, 230–237. https://doi.org/10.1016/j.foodchem.2017.12.043.

Tuntoolavest, M., Burgos, W.D., 2005. Anaerobic phenol oxidation by *Geobacter metallireducens* using various electron acceptors. Environ. Eng. Sci. 22, 421–426. https://doi.org/10.1089/ees.2005.22.421.

Ueki, T., 2021. Cytochromes in extracellular electron transfer in *Geobacter*. Appl. Environ. Microbiol. 87 https://doi.org/10.1128/aem.03109-20.

Wang, Y., Wen, Q., Chen, Y., Li, W., 2020. Conductive polypyrrole-carboxymethyl cellulose-titanium nitride/carbon brush hydrogels as bioanodes for enhanced energy output in microbial fuel cells. Energy 204, 117942. https://doi.org/10.1016/j.energy.2020.117942.

Wen, H., Zhu, H., Yan, B., Xu, Y., Shutes, B., 2020. Treatment of typical antibiotics in constructed wetlands integrated with microbial fuel cells: roles of plant and circuit operation mode. Chemosphere 250, 126252. https://doi.org/10.1016/j.chemosphere.2020.126252.

Xiao, L., Wang, Y., Lichtfouse, E., Li, Z., Kumar, P.S., Liu, J., Feng, D., Yang, Q., Liu, F., 2021a. Effect of antibiotics on the microbial efficiency of anaerobic digestion of wastewater: a review. Front. Microbiol. https://doi.org/10.3389/fmicb.2020.611613.

Xiao, L., Li, J., Lichtfouse, E., Li, Z., Wang, Q., Liu, F., 2021b. Augmentation of chloramphenicol degradation by *Geobacter*-based biocatalysis and electric field. J. Hazard Mater. 410, 124977. https://doi.org/10.1016/j.jhazmat.2020.124977.

Xiao, L., Lichtfouse, E., Kumar, P.S., 2021c. Advantage of conductive materials on interspecies electron transfer-independent acetoclastic methanogenesis: A critical review. Fuel 306, 121577. https://doi.org/10.1016/j.fuel.2021.121577.

Xiao, L., Lichtfouse, E., Kumar, S., Wang, Q., Liu, F., 2021d. Biochar promotes methane production during anaerobic digestion of organic waste. Environ. Chem. Lett. https://doi.org/10.1007/s10311-021-01251-6.

Xiao, L., Zheng, S., Lichtfouse, E., Luo, M., Tan, Y., Liu, F., 2020a. Carbon nanotubes accelerate acetoclastic methanogenesis: from pure cultures to anaerobic soils. Soil Biol. Biochem. 150, 107938. https://doi.org/10.1016/j.soilbio.2020.107938.

Xiao, L., Liu, F., Lichtfouse, E., Zhang, P., Feng, D., Li, F., 2020b. Methane production by acetate dismutation stimulated by *Shewanella oneidensis* and carbon materials: an alternative to classical CO_2 reduction. Chem. Eng. J. 389, 124469. https://doi.org/10.1016/j.cej.2020.124469.

Xiao, L., Wei, W., Luo, M., Xu, H., Feng, D., Yu, J., Huang, J., Liu, F., 2019a. A potential contribution of a Fe(III)-rich red clay horizon to methane release: biogenetic magnetite-mediated methanogenesis. Catena 181, 104081. https://doi.org/10.1016/j.catena.2019.104081.

Xiao, L., Sun, R., Zhang, P., Zheng, S.L., Tan, Y., Li, J.J., Zhang, Y.C., Liu, F.H., 2019b. Simultaneous intensification of direct acetate cleavage and CO2 reduction to generate methane by bioaugmentation and increased electron transfer. Chem. Eng. J. 378, 122229. https://doi.org/10.1016/j.cej.2019.122229.

Xiao, L., Liu, F., Liu, J., Li, J., Zhang, Y., Yu, J., Wang, O., 2018. Nano-Fe_3O_4 particles accelerating electromethanogenesis on an hour-long timescale in wetland soil. Environ. Sci.: Nano 5, 436–445. https://doi.org/10.1039/c7en00577f.

Xing, L., Wang, Z., Gu, M., Yin, Q., Wu, G., 2020. Coupled effects of ferroferric oxide supplement and ethanol co-metabolism on the methanogenic oxidation of propionate. Sci. Total Environ. 723, 137992. https://doi.org/10.1016/j.scitotenv.2020.137992.

Xu, H.D., Xiao, L.L., Zheng, S.L., Zhang, Y.C., Li, J.J., Liu, F.H., 2019. Reductive degradation of chloramphenicol by *Geobacter metallireducens*. Sci. China Technol. Sci. 62, 1688–1694. https://doi.org/10.1007/s11431-018-9415-2.

Yan, Weifu, Xiao, Y., Yan, Weida, Ding, R., Wang, S., Zhao, F., 2019. The effect of bioelectrochemical systems on antibiotics removal and antibiotic resistance genes: a review. Chem. Eng. J. https://doi.org/10.1016/j.cej.2018.10.128.

Yang, C.W., Liu, C., Chang, B.V., 2020a. Biodegradation of amoxicillin, tetracyclines and sulfonamides in wastewater sludge. Water 12, 2147. https://doi.org/10.3390/w12082147.

Yang, J., Ji, G., Gao, Y., Fu, W., Irfan, M., Mu, L., Zhang, Y., Li, A., 2020b. High-yield and high-performance porous biochar produced from pyrolysis of peanut shell with low-dose ammonium polyphosphate for chloramphenicol adsorption. J. Clean. Prod. 264, 121516. https://doi.org/10.1016/j.jclepro.2020.121516.

Yang, K., Ji, M., Liang, B., Zhao, Y., Zhai, S., Ma, Z., Yang, Z., 2020c. Bioelectrochemical degradation of monoaromatic compounds: current advances and challenges. J. Hazard Mater. https://doi.org/10.1016/j.jhazmat.2020.122892.

Zhang, T., Tremblay, P.L., Chaurasia, A.K., Smith, J.A., Bain, T.S., Lovley, D.R., 2013. Anaerobic benzene oxidation via phenol in *Geobacter metallireducens*. Appl. Environ. Microbiol. 79, 7800–7806. https://doi.org/10.1128/aem.03134-13.

Zhang, S., Song, H.L., Yang, X.L., Li, H., Wang, Y.W., 2018. A system composed of a biofilm electrode reactor and a microbial fuel cell-constructed wetland exhibited efficient sulfamethoxazole removal but induced sul genes. Bioresour. Technol. 256, 224–231. https://doi.org/10.1016/j.biortech.2018.02.023.

Zheng, T., Li, J., Ji, Y., Zhang, W., Fang, Y., Xin, F., Dong, W., Wei, P., Ma, J., Jiang, M., 2020. Progress and prospects of bioelectrochemical systems: electron transfer and its applications in the microbial metabolism. Front. Bioeng. Biotechnol. https://doi.org/10.3389/fbioe.2020.00010.